

CapsFlow: Optical Flow Estimation with Capsule Networks

Rajat Arora*, Rahul Chand*, K Ram Prabhrakar and R Venkatesh Babu

Video Analytics Lab, Indian Institute of Science

Abstract

We present a framework to use recently introduced Capsule Networks for solving the problem of Optical Flow, one of the fundamental computer vision tasks. Most of the existing state of the art deep architectures either uses a correlation operation to match features from them. While correlation layer is sensitive to the choice of hyperparameters and does not put a prior on the underlying structure of the object, spatio temporal features will be limited by the network’s receptive field. Also, we as humans look at moving objects as whole, something which cannot be encoded by correlation or spatio temporal features. Capsules, on the other hand, are specialized to model separate entities and their pose as a continuous matrix. Thus, we show that a simpler linear operation over poses of the objects detected by the capsules is enough to model flow. We show results on a small toy dataset where we outperform FlowNetC and PWC-Net models.

1 Introduction

Optical flow estimation is a fundamental computer vision problem. Given a pair of images, optical flow attempts to find dense motion field, assigning a vector displacement indicating where they moved to in the second image. Estimating the displacement field between the two images requires learning both the finer local details as well as the global structural information to match them at different locations

In recent years, great progress has been achieved in estimating the optical flow using deep learning methods (Fischer et al., 2015; Ilg et al., 2016; Meister et al., 2017; Sun et al., 2017). Although existing approaches have achieved good performance, most methods rely on a multi-stage pipeline and calculation of correlation map or learning spatio-temporal features between image

features to aid the matching process. Correlation typically works by calculating correspondences between a set of pixels within a given neighborhood, for a particular search space.

Formally, given two feature maps f_1, f_2 with w, c, h being their width, height and number of channels, correlation layer compares each patch from f_1 with each patch from f_2 in a fixed neighbourhood. The size of the patch (\mathbf{K}) is equal to $2k + 1$, where k is the kernel size. Also for reducing complexity, all patches are not matched. A patch centered at x_1 in f_1 is only correlated with patches in f_2 whose center x_2 lies in the neighbourhood whose size is $2d + 1$ and is centered at x_1 , where d is the displacement parameter. The complexity of the operation is D^2cwh , and the output is of size $(w \times h \times D^2)$.

Thus, depending upon these hyper-parameters correlation may or may not be able to find an exact match. Similarly, learning spatio-temporal features would be limited by the receptive field of the filters used. Capsules on other hand are naturally suited to this task as position and orientation of any entity captured by a particular capsule is represented by a continuous motion vector which can model various types of complex rigid or non-rigid motion. To this end, we show the effectiveness of capsules on a toy dataset and also present first work, to the best of our knowledge, to extend capsules to dense prediction tasks.

2 Related Work

Capsule Networks: Capsule Networks introduced by (Sabour et al., 2017) are an alternative neural net architecture as compared to Convolutional Neural Networks (CNN) that aim for view-point equivariance rather than invariance. Capsule Networks do so by using a group of neurons, called capsules, to encode both the presence as well pose of the entity with respect to the viewer. Furthermore, they use a dynamic routing mecha-

Draft was completed as part of undergraduate thesis & submitted to WACV 2019

nism to transform poses from one capsule layer to the next

Though initially, capsule networks used a single 8- dimensional vector to encode pose of an entity with its norm representing the probability of its presence, it was later modified by (Hinton et al., 2018) to use a 4x4 matrix to represent entity’s pose and a separate scalar to denote presence. (Hinton et al., 2018) also replaced routing by agreement in (Sabour et al., 2017) with EM based routing. Since their introduction, capsules have been used for binary segmentation (LaLonde and Bagci, 2018), Action Recognition (Duarte et al., 2018), 3D point reconstruction (Zhao et al., 2018) and many other applications.

Optical Flow Methods: Classically, the optical flow was estimated via energy minimization methods, particularly after the work of (Horn and Schunck, 1981). However, energy minimization methods fail to work for large displacement ((Brox et al., 2004)) and a series of works ((Barnes et al., 2010; Liu et al., 2011; Xu et al., 2012)) use descriptor or feature matching in conjunction with energy minimization, carried out in a coarse-to-fine manner, to alleviate the problem. (Weinzaepfel et al., 2013) blended the aforementioned work with deep learning, using manually selected convolutional filters to extract features at multiple scales before energy minimization

CNNs have become ubiquitous for high-level vision problems and optical flow computation is no exception. (Fischer et al., 2015) introduced FlowNetC, which used a correlation over a set of learned features and refines it using CNN layers in a multi-scale fashion. SpyNet (Ranjan and Black, 2016) stacks both the input images together to learn spatio-temporal filters at multiple-scales and learns residual flow to hierarchically refine the output. PWC-Net (Sun et al., 2017) combines the two by using the correlation between learned features to get an estimate of the disparity at multiple scales, followed by hierarchical refinement to produce the final flow. Also, as getting real-world data for optical flow is a difficult task, (Meister et al., 2017; Wang et al., 2017; Zou et al., 2018) have explored unsupervised methods for the task and build on FlowNetC’s architecture and use bidirectional warping based loss along with additional smoothness constraints to achieve satisfactory performance.

Our work is a departure from this basic tem-

plate as we try to leverage the better representational capability of capsule networks, owing to the presence of a motion vector, to implicitly model different kinds of transformations an object may undergo.

3 Overall Approach

Intuition: A single neuron in a CNN captures the presence or absence of a feature in the image, on the other hand, a single capsule captures not only the existence of an entity but also outputs a 4x4 pose matrix which can learn the spatial relationship (translation, rotation, etc.) of an entity with respect to the viewer. We utilize this property by calculating the motion of an entity (object) as a transformation between its pose matrices. This reduces the computationally expensive correlation layer into a single operation. The intuition for the reformulation is that the pose matrix of a capsule is capable of learning positional parameters of the entity it describes, therefore using a suitable transformation (like subtracting the pose matrix for two images) one could capture how an entity moved between two images

Capsules are ideally more suited to classification tasks since each class capsule tries to model a separate entity. But, real-world scenes and similarly traditional optical flow datasets do not have a setlist of classes. We thus show the effectiveness of capsule networks in case of class supervision by using a toy dataset consisting of five different shapes (or classes) of varying sizes and orientation as shown in Figure 3.

3.1 Capsule network

Before we explain our CapFlow architecture, we briefly explain the main components of a standard Capsule Network:

Convolutional encoder: Capsule networks use few convolutional layers along with ReLU activation to extract basic features from the inputs. These features are then used as input to primary capsule layers.

Capsule Layers: The output from the convolutional layers is individually passed to a set of capsules, which perform a convolution to output a 4x4 transformation matrix, M , representing pose of the detected entity and an activation probability, A . The output from the primary capsules is then routed into secondary capsule layers using a trainable transformation matrix W between each

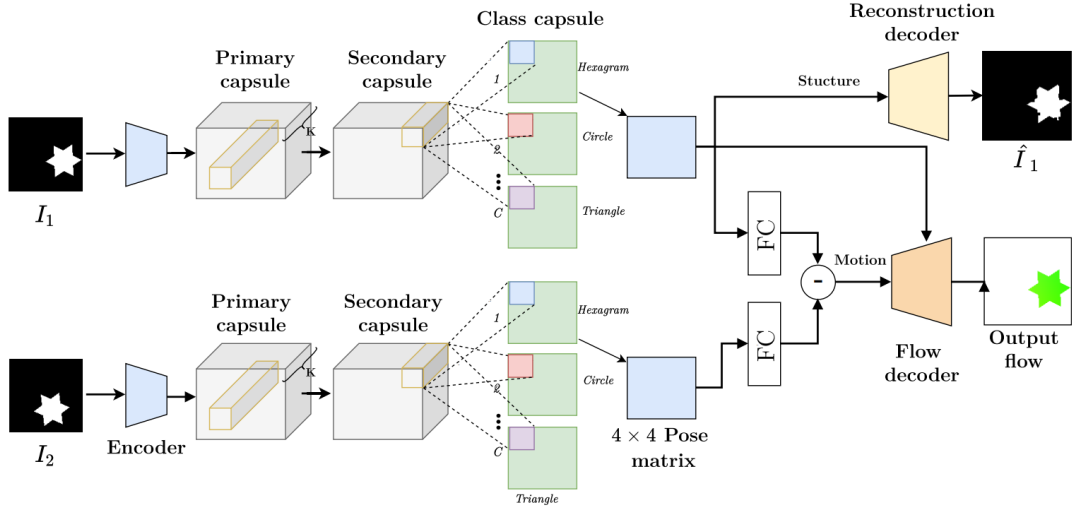


Figure 1: First part of the architecture consists of a Siamese network where a pair of input images, Image 1 (I_1) and Image 2 (I_2), are passed through a convolutional encoder. Followed by 3 layers of capsules (including class capsules) to output a 4×4 pose matrix for each of the C ($=5$) possible classes. We select the matrices belonging to the classes with the highest average activation for both images. Then, the two encodings are passed through FC layers to form richer embeddings. We then subtract the two embeddings to get a motion embedding which is then passed to a convolutional decoder to get the output flow map. Pose matrices from the first image are also passed as skip connection to flow decoder to refine the flow. The pose matrices are also used to reconstruct back the input image I_1 which acts as a regularizer.

pair of capsules of consecutive layers. A pose matrix of capsule i , in layer L , is multiplied by W_{ij} to yield $V_{ij} = M_i W_{ij}$ which represents its vote for the j^{th} capsule in layer $L + 1$. The poses in $L + 1$ th layer then uses a non-linear routing mechanism (explained next) to determine its poses and activation vector. Final capsule layer consists of a single capsule representing the final classification label.

Routing between Capsules: Each of the element in 4×4 pose matrix of the parent capsule belongs to a Gaussian distribution whose parameters are estimated using the Expectation-Maximization (EM) algorithm. Broadly, Expectation step attempts at calculating the probability that each of the capsules in layer L is explained by capsules in layer $L + 1$. Maximization step then tries to maximize the activation of a given capsule in layer $L + 1$ depending on inputs from layer L .

3.2 CapsFlow network architecture

The overview of Siamese CapsFlow architecture is shown in Figure 1. The input to the network is a pair of $128 \times 128 \times 3$ RGB images, I_1 and I_2 . The network begins with four convolutional layers with a kernel size of 3×3 and strides of 2 and 1 alternatively, each with a ReLU non-

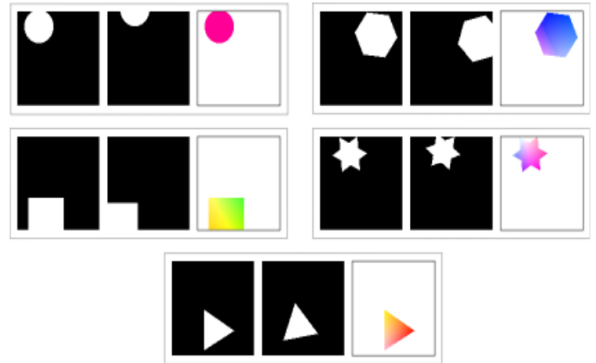


Figure 2: Examples of input images and the ground truth flow used for training and validation.

linearity. The resulting feature map of dimension $32 \times 32 \times 256$ is transformed into a capsule layer of dimension $16 \times 16 \times 16 \times 17$, ($K \times H \times W \times 4 * 4 + 1$, where K =number of capsule types) by applying a 3×3 convolutional operation with stride 2. This is followed by a second capsule layer with 16 capsule types and a 7×7 receptive field with stride 2.

The second capsule layer is then connected to a final convolutional capsule layer (class capsule) with C capsule types, where C is the number of shapes in the dataset. The resulting output ($C \times 6 \times 6 \times (16 + 1)$) consists of two components, a

pose matrix ($C \times 6 \times 6 \times 16$) and an activation vector ($C \times 6 \times 6 \times 1$). Note that, we do not perform coordinate addition to calculate the poses and activations of the final capsule layer since the penultimate and final capsule layers are not fully connected therefore there is no loss of spatial information ((Hinton et al., 2018; Duarte et al., 2018)). Coordinate addition is required when routing from a 2D capsule layer ($C \times H \times W \times 17$) to a 1D capsule ($C \times 17$) to preserve spatial information. The activation probability for each shape is calculated by averaging over the spatial dimensions (6×6) of the shape’s activation vector. The capsule with the highest activation probability corresponds to the shape predicted by network.

The output pose of the class capsule layer ($C \times 6 \times 6 \times 16$) is then masked to obtain the pose matrix corresponding to the ground truth shape. During training, we use the knowledge of ground truth to choose the correct class while during inference the class is chosen based on the highest mean activation vector. The masked output ($6 \times 6 \times 16$) is passed to a fully connected layer with RELU non-linearity to obtain structural embedding of shape ($8 \times 8 \times 16$). The structure embeddings for both I_1 and I_2 are passed to a shared convolutional layer and then subtracted to calculate the motion embedding, which encodes the motion from I_1 to I_2 .

To help the network learn the correct pose parameters, we pass the structure embedding to a four layer transposed convolutional decoder to reconstruct the input image, I_1 . This is necessary since training without a reconstruction decoder results in the network learning a sub-par structure embedding, which in turn affects the motion embedding. To construct the final flow map, both the motion and structure embedding are passed to a decoder consisting of four transposed convolutional layers each with stride 2 and kernel size of 4×4 . The output of the decoder ($64 \times 64 \times 2$) is extrapolated to obtain the predicted optical flow map of shape $128 \times 128 \times 2$.

3.3 Objective Function

The objective function is made of three losses: a) Mean squared reconstruction loss to learn the correct pose embedding, b) Activation loss to learn the correct target class, and c) End-Point-Error (EPE) loss between ground truth flow map and predicted flow map. To calculate reconstruction loss, we compute mean square error between I_1

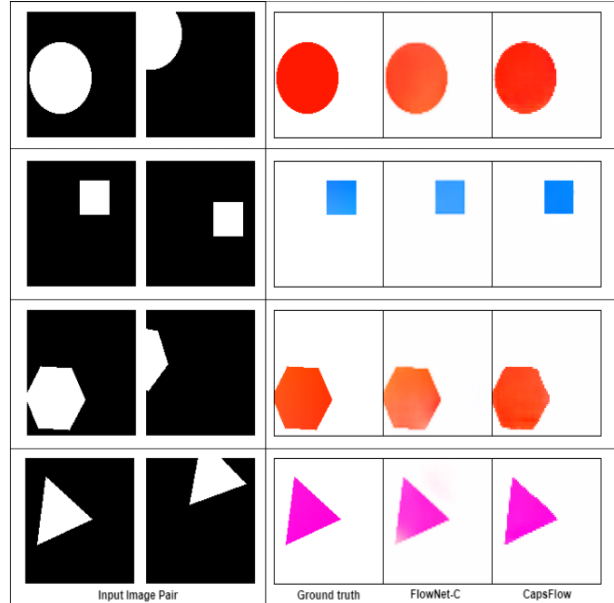


Figure 3: Few examples indicating FlowNetC underestimating flow while output of our proposed model is much closer to ground truth. (Best seen in color and zoomed in.)

and reconstructed image \hat{I}_1 .

$$L_{mse} = ||I_1 - \hat{I}_1||^2$$

Empirically, we found that reconstruction loss acts as a regularizer and helps ensure that the pose matrix learns all the relevant features. In absence of reconstruction loss, the network does not converge, probably due to the reason that there is not enough supervision to learn correct pose matrices (flow depends only on their difference and not actual values). We use margin loss to train the activation vector and is calculated as,

$$L_m = \sum_{i \neq t} \max[0, m - (\text{mean}(a_t) - \text{mean}(a_i))]^2$$

where a_t is the activation of the target shape class and a_i is the activation corresponding to capsule i . We take the mean of the activation before computing the loss. The capsule with the highest activation is used at test stage to determine the poses to be subtracted to estimate flow. The margin m is set to 0.95 during training. EPE loss is calculated as

$$L_{epe} = ||flow_{gt} - flow_{pred}||^2$$

Thus, CapsFlow network is trained using the following objective function

$$L = L_{epe} + \lambda_1 L_{margin} + \lambda_2 L_{mse}$$

Encoder					
Conv Stride	3x3	3x3	3x3	3x3	
No.of filters	2	1	2	1	
BatchNorm	Yes	Yes	Yes	Yes	
Decoder					
Transpose Conv	4x4	4x4	4x4	-	-
Convolution	-	-	-	1x1	1x1
Stride	2	2	2	1	1
No.of filters	64	64	32	16	2
Reconstruction Decoder					
Transpose Conv	4x4	4x4	4x4	4x4	-
Convolution	-	-	-	-	1x1
Stride	2	2	2	1	1
No.of filters	32	64	16	8	1

Table 1: CapsFlow network architecture

4 Experiments

To check the effectiveness of our approach we prepare a toy dataset consisting of simple shapes as shown in Figure 3 and compare our method to FlowNetC (Fischer et al., 2015) as well as PWC-Net (Sun et al., 2017). We also explore ways to extend our method to real-world images by experimenting on Flying Chairs dataset

4.1 Training

The data is generated by sampling a random shape type (square, hexagon, triangle, circle, and hexagram), and a random (x, y) location between 0 to 128. The shape is then randomly rotated and translated to obtain the corresponding second image. The data is generated on-fly to prevent overfitting. We have a fixed set of 2500 images used for testing. The architecture details of encoder and decoders used is provided in Table 1.

The reconstruction and flow decoder can either be trained simultaneously or sequentially, starting with first with reconstruction and then flow. The values of λ_1 and λ_2 in equation 4 are chosen to be 0.05 and 2.5 respectively. All models were trained on an NVIDIA GTX 1080Ti GPU. CapsFlow was trained for a total of 30K iterations with a mini-batch size of 64. For sequential case, the reconstruction decoder was first pretrained for 10k iterations. The number of EM iterations during routing was set to 3 as in (Hinton et al., 2018). We used Adam optimizer (Kingma and Ba, 2014) with a fixed learning rate of 0.001.

Model	EPE	Params(in M)	Time(ms)
CapsFlow (T)	0.48	1.62	13.39
CapsFlow (S)	0.39	1.62	13.39
FlowNetC	0.50	39.17	3.1
PWC-Net	0.47	8.75	12.1

Table 2: Quantitative comparison on single shape dataset: T & S refers to simultaneous and sequential training respectively, for more information refer to Section 4.1. The average time is calculated for an input pair of resolution 128x128. The best result is highlighted in red color, while the second-best in blue color.

4.2 Results

We compare our results with FlowNetC and PWC-Net. Both of these models were trained using End Point Error for 90k iterations with a batch size of 16, using Adam Optimizer with learning rate 0.001, similar to proposed CapsFlow. The end-point error comparison for both CapsFlow models is shown in Table 2. Both variants of CapsFlow form better than both FlowNetC and PWC-Net while having 8x fewer parameters. But, despite lower number of parameters, capsules take significantly more time primarily due to iterative EM routing procedure. But as capsule networks develop and see wider adoption there is a high likelihood that hardware acceleration and better routing procedures will be able to reduce the time overhead.

On visualizing flow outputs for CapsFlow and FlowNetC, we notice that latter underestimates flow magnitude for a large number of samples as shown in Figure 3. To confirm this, we test both models on another validation set having an average flow magnitude 1.5 times more than that of the training set. FlowNetC saw a 3x jump in the EPE from 0.50 to 1.51 on this new set while CapsFlow EPE only increased from 0.39 to 0.81. This highlights a higher generalization capacity of CapsFlow. We hypothesize the reason for this observation to be the fact that while capsules model flow as a continuous motion matrix, correlation is sensitive to the choice of displacement and neighborhood size and thus may not be able to model the large magnitude of flows as well, particularly if they were not seen during training. We also try to see what pose matrices and the difference matrix model by scaling their magnitude uniformly in the range $[-1, 1]$ in with increments of 0.5. On changing the magnitude of the difference we see the flow

changing from one extreme in the flow spectrum to total opposite but no change in overall structure (Figure 4). On the other hand, the changing magnitude of skip connection in the range [0.25, 2.5] in increments of 0.25; changes the scale of the shape as shown in Figure 5. This shows that flow and pose are essentially getting disentangled with the flow coming from the difference of poses while structure comes from Image 1’s pose matrix.

Extending to multiple shapes: We generate instances of our MultiShape dataset by sampling two different shapes on-fly for each image. The flow for both shapes is combined to produce the ground truth flow map. On average, the bounding box for each shape is of size 50×50, and the center of both shapes is bounded inside a region of size 90×90. Therefore the bounding boxes for both shapes on average have a 45% overlap.

While training CapsFlow on multiple shapes we mask one class capsule at a time and use its pose matrix to construct the corresponding flow map. The final output of the network is obtained by superimposing both flow maps (in regions where both maps intersect, we consider the flow of only one shape based on the same priority that was used for creating the training set). The training parameters and losses for this experiment are the same as those for a single shape. We achieve a marginally better EPE of 1.78 as compared to FlowNetC’s, 1.9. For test images, we pick the two most active class capsules and use their pose matrices to construct the individual flow map (which are later used to find the final flow map). One advantage of CapsFlow is that unlike other methods we can obtain the individual flow maps for each shape in the image. Since capsules enforce a strong constraint on shapes of each object, even in cases where one of the shapes is highly occluded, CapsFlow can extrapolate the whole object using its prior about the shape of the object as shown in Figure 6.

4.3 Unsupervised Training

We also attempt to test the effectiveness of the proposed model in an unsupervised setting. To train CapsFlow in an unsupervised setting, we average the outputs of all the capsules in the final layer, rather than masking them. We train CapsFlow using the same set of losses used in UnFlow [(Meister et al., 2017)], the losses are a) occlusion-aware photometric loss between the input images and their flow warped counterparts, b) second-order

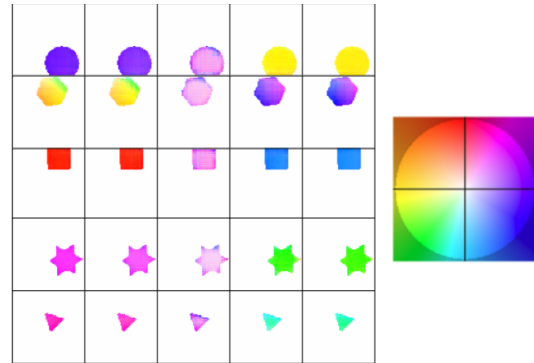


Figure 4: *Left:* Results from interpolating flow. We scale the magnitude of difference matrix between the poses of given images while keeping the skip connection from I_1 same and notice that difference matrix only changes the flow without any change in structure. To be precise, scaling magnitude seems to be equivalent to moving from one end of flow spectrum to diametrically opposite. *Right:* Optical flow color coding.

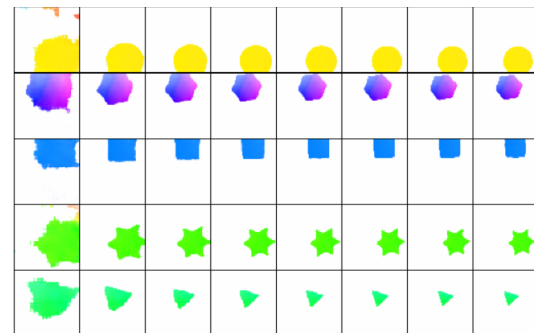


Figure 5: We change the magnitude of the pose matrix from I_1 without changing the difference and notice only the output shape of the flow changes without any change to flow values.

smoothness constraint to encourage co-linearity of neighboring flows, and c) forward-backward consistency penalty. Our model performs comparably to UnFlow method in shapes dataset with an EPE of 2.05 as compared to UnFlow method EPE of 1.8. But, despite good EPE score, we notice that in the absence of masking, only 1 out of the 5 classes ever remain active and comparable results can be achieved if other capsules are not considered. The reason for this is elaborated in the next section

5 Drawbacks and Future Work

Though our proposed model gave promising results on a toy dataset, capsule network still cannot be naively used on real world samples. Capsules tend to perform poorly in tasks where latent capsules do not represent distinct classes [13]. The sub-par performance is due to capsules learning

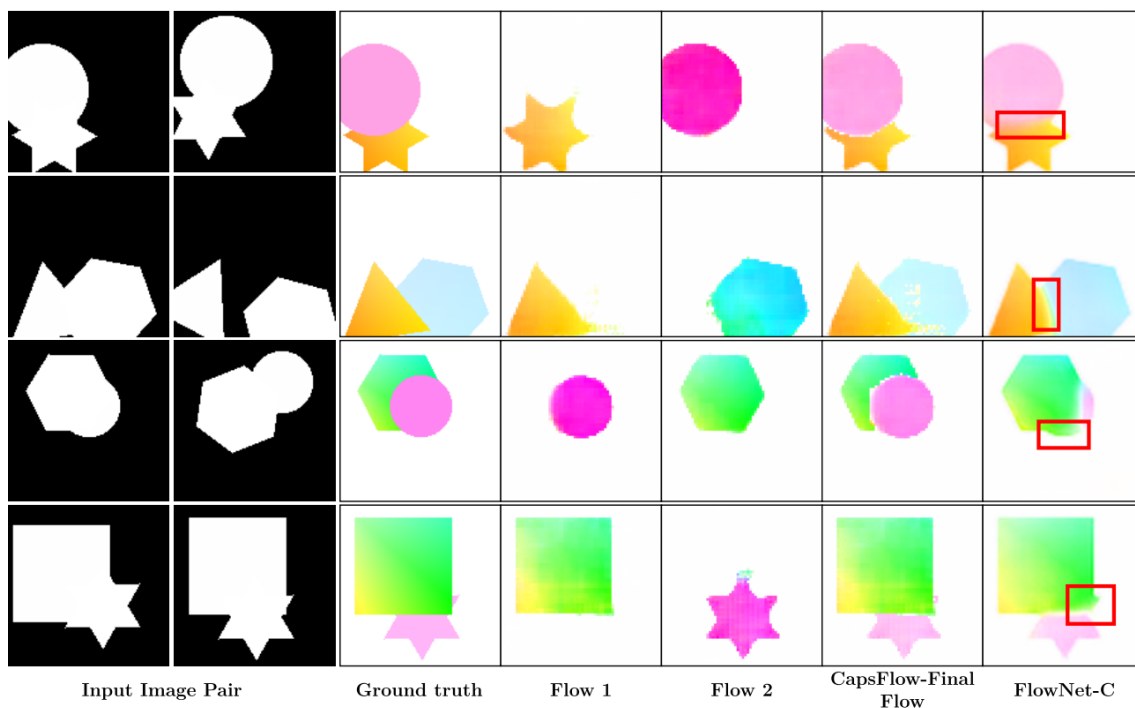


Figure 6: CapsFlow can successfully model individual flows even in case of high overlap. Also, at motion boundaries and overlapping regions, FlowNetC expectedly in absence of any prior on shape boundaries, assigns flow belonging to one shape to another (highlighted in the red box)

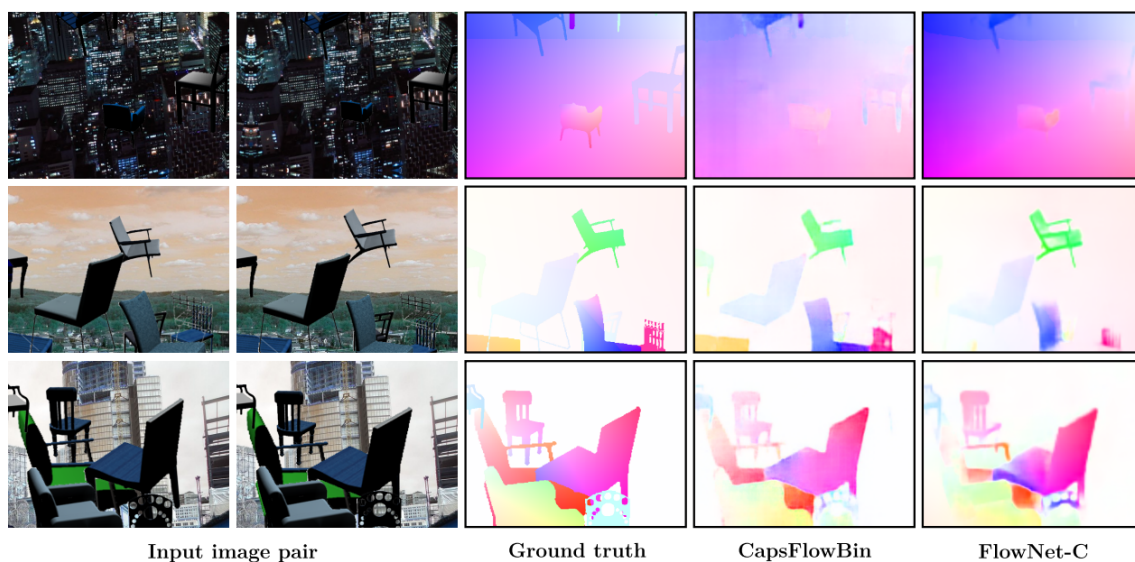


Figure 7: Qualitative results on FlyingChairs dataset. Our CapsFlowBin (CapsFlow with binning) method obtained EPE of 3.6, while FlowNetC achieves EPE of 2.0.

parameters using different paradigms. Rather than learning all parameters using EM-routing (generatively), capsules learn transformation matrices in a discriminative fashion through back-propagation in the absence of which we may get degenerate solutions, such as when all transformation matrices collapsing to zero

Without concrete class capsules, transformation matrices have no incentive or gradient to differ from each other. In this case, the probability that a particular subset of lower level capsules are transformed into similar clusters in the pose space of two higher-level capsules j and k increases. This results in a breakdown in the part-to-whole relationship as both j and k now model very similar entities, which in turn results in lower level capsules that route to j and k to model similar entities too [(Rawlinson et al., 2018)]. Therefore unmasked latent capsule networks require exponentially more capsules than their masked counterpart. This is a major shortcoming as such a requirement is very restrictive since the majority of dense prediction tasks have no (definite or explicit) classes/entities, e.g. Depth estimation, Super-resolution, 3D segmentation. Another drawback of capsule networks is that, unless explicitly trained, each class capsule models only single instance of that entity, thus will fail in cases there are multiple instances of same entity in a scene. Further capsules also cannot model global motion though that is not a major issue as there are other robust techniques available to estimate camera motion.

One work-around for dense optical flow that we tried was to spatially bin the ground truth and treat those bins as class capsules. The input to these class capsules was obtained by subtracting poses from secondary capsule layer itself. This technique gave good results during training but fails during testing due to high mis-classification rate (See Figure 7).

But despite these drawbacks capsules seem to be a promising direction for future research and can address the drawbacks faced by current CNN based deep methods in tracking and optical flow computation.

6 Conclusion

From the experiments discussed above, we conclude that Capsule Networks, despite various weaknesses and still being in infancy, offer a great

way for modeling motion and calculating optical flow. Though they outperform the current state of the art on a toy dataset for both single and multiple shapes scenarios and also demonstrate higher generalizability, they require more research to make them adapt to cases where a comprehensive list of entities may not be available or if there are multiple instances of the same entity is present in the scene. But despite that, we believe Capsule Network, due to their greater representational capacity and implicit encoding of spatial relationships between objects, are an exciting direction for further research on motion estimation and optical flow. We think that with further improvements in Capsule Networks, our framework can be adapted to obtain better results on real-world images.

References

- Connelly Barnes, Eli Shechtman, Dan B. Goldman, and Adam Finkelstein. 2010. The generalized patchmatch correspondence algorithm. In *European Conference on Computer Vision*.
- Thomas Brox, Andrés Bruhn, Nils Papenberg, and Joachim Weickert. 2004. High accuracy optical flow estimation based on a theory for warping. In *European Conference on Computer Vision*.
- Kevin Duarte, Yogesh Singh Rawat, and Mubarak Shah. 2018. Videocapsulenet: A simplified network for action detection. In *Neural Information Processing Systems*.
- Philipp Fischer, Alexey Dosovitskiy, Eddy Ilg, Philip Häusser, Caner Hazirbas, Vladimir Golkov, Patrick van der Smagt, Daniel Cremers, and Thomas Brox. 2015. [Flownet: Learning optical flow with convolutional networks](#). *CoRR*, abs/1504.06852.
- Geoffrey E. Hinton, Sara Sabour, and Nicholas Frosst. 2018. Matrix capsules with em routing. In *International Conference on Learning Representations*.
- Berthold K.P. Horn and Brian G. Schunck. 1981. [Determining optical flow](#). *Artificial Intelligence*, 17(1):185–203.
- Eddy Ilg, Nikolaus Mayer, Tonmoy Saikia, Margret Keuper, Alexey Dosovitskiy, and Thomas

- Brox. 2016. [FlowNet 2.0: Evolution of optical flow estimation with deep networks](#). *CoRR*, abs/1612.01925.
- Diederik P. Kingma and Jimmy Ba. 2014. Adam: A method for stochastic optimization. *CoRR*, abs/1412.6980.
- Rodney LaLonde and Ulas Bagci. 2018. Capsules for object segmentation. *ArXiv*, abs/1804.04241.
- Ce Liu, Jenny Yuen, and Antonio Torralba. 2011. [Sift flow: Dense correspondence across scenes and its applications](#). *IEEE Transactions on Pattern Analysis and Machine Intelligence*, 33(5):978–994.
- Simon Meister, Junhwa Hur, and Stefan Roth. 2017. Unflow: Unsupervised learning of optical flow with a bidirectional census loss. In *AAAI Conference on Artificial Intelligence*.
- Anurag Ranjan and Michael J. Black. 2016. Optical flow estimation using a spatial pyramid network. *2017 IEEE Conference on Computer Vision and Pattern Recognition (CVPR)*, pages 2720–2729.
- David Rawlinson, Abdelrahman Ahmed, and Gideon Kowadlo. 2018. Sparse unsupervised capsules generalize better. *ArXiv*, abs/1804.06094.
- Sara Sabour, Nicholas Frosst, and Geoffrey E. Hinton. 2017. Dynamic routing between capsules. *ArXiv*, abs/1710.09829.
- Deqing Sun, Xiaodong Yang, Ming-Yu Liu, and Jan Kautz. 2017. Pwc-net: Cnns for optical flow using pyramid, warping, and cost volume. *2018 IEEE/CVF Conference on Computer Vision and Pattern Recognition*, pages 8934–8943.
- Yang Wang, Yezhou Yang, Zhenheng Yang, Liang Zhao, and Wei Xu. 2017. Occlusion aware unsupervised learning of optical flow. *2018 IEEE/CVF Conference on Computer Vision and Pattern Recognition*, pages 4884–4893.
- Philippe Weinzaepfel, Jérôme Revaud, Zaïd Harchaoui, and Cordelia Schmid. 2013. Deep-flow: Large displacement optical flow with deep matching. *2013 IEEE International Conference on Computer Vision*, pages 1385–1392.
- Li Xu, Jiaya Jia, and Yasuyuki Matsushita. 2012. Motion detail preserving optical flow estimation. *IEEE Transactions on Pattern Analysis and Machine Intelligence*, 34(9):1744–1757.
- Yongheng Zhao, Tolga Birdal, Haowen Deng, and Federico Tombari. 2018. [3d point-capsule networks](#). *CoRR*, abs/1812.10775.
- Yuliang Zou, Zelun Luo, and Jia-Bin Huang. 2018. [Df-net: Unsupervised joint learning of depth and flow using cross-task consistency](#). *CoRR*, abs/1809.01649.